Single-molecule diffusivity quantification unveils ubiquitous net charge-driven

protein-protein interaction

Alexander A. Choi, Ke Xu*

Department of Chemistry, University of California, Berkeley, California 94720, United States

* Corresponding author: xuk@berkeley.edu (K.X.)

Abstract

Recent microscopy and NMR studies have noticed substantial suppression of intracellular diffusion for

positively charged proteins, suggesting an overlooked role of electrostatic attraction in nonspecific protein

interactions in the predominantly negatively charged intracellular environment. Utilizing single-molecule

detection and statistics, here we quantify in aqueous solutions how protein diffusion, in the limit of low

diffuser concentration to avoid aggregate/coacervate formation, is modulated by differently charged

interactor proteins over wide concentration ranges. We thus report substantially suppressed diffusion when

oppositely charged interactors are added at ppm levels, yet unvaried diffusivities when same-charge

interactors are added beyond 1%. The electrostatic attraction-driven suppression of diffusion is sensitive

to the protein net charge states, as probed by varying the solution pH and ionic strength or chemically

modifying the proteins, and is robust across different diffuser-interactor pairs. By converting the measured

diffusivities to diffuser diameters, we further show that in the limit of excess interactors, a positively

charged diffuser molecule effectively drags along just one monolayer of negatively charged interactors,

where further interactions stop. We thus unveil ubiquitous, net charge-driven protein-protein interactions

and shed new light on the mechanism of charge-based diffusion suppression in the living cell.

1

Introduction

Molecular diffusion stands as a fundamental process of the cell while also providing a valuable window into intermolecular interactions.¹⁻⁴ We recently developed single-molecule displacement/diffusivity mapping (SMdM),⁵ in which the mass statistics of transient (~<1 ms) single-molecule displacements enables the quantification of molecular translational diffusion *in vitro*⁶⁻⁹ and in the living cell.^{5,7,10,11} For fluorescent proteins (FPs) expressed in the mammalian cell, SMdM unexpectedly unveils the protein net charge as a key determinant of their diffusivity. Intriguingly, across diverse cytoplasmic, nuclear, and intraorganellar environments, the possession of positive, but not negative, net charges substantially impedes diffusion.^{5,11} These results echo other recent microscopy and NMR observations in bacterial and mammalian cells generally showing slower diffusion for positively charged proteins.¹²⁻¹⁶

Our analysis of the net charges of major proteins in the mammalian cell (per mass spectrometry-detected abundances^{17,18}) shows an excessive preponderance of negative values.^{5,11} Combined with the known high abundance of intracellular small cations (~150 mM) but low availability of small anions (~20 mM),¹⁹⁻²¹ we thus reason that in the mammalian cytoplasm, positive charges are predominantly carried by small ions, whereas negative charges are mainly carried by RNA and proteins (**Table S1**). Consequently, it is plausible that in the mammalian cell, positively charged proteins will be dragged by the predominantly negatively charged intracellular macromolecules, thus explaining the above experimental observations of charge-sign asymmetric impediment of diffusion.

However, the above model, which would imply strong ubiquitous net charge-driven protein-protein interactions in intracellular environments, has yet to be validated experimentally or recapitulated *in vitro*. As intracellular proteins are predominantly negatively charged, protein-induced macromolecular crowding²²⁻²⁴ is often examined between proteins of the same, negative charge sign. Meanwhile, oppositely charged biomacromolecules have been mixed at near equimolar ratios at high (>~0.1 wt% or >~10 μ M) concentrations to generate polyelectrolyte complexes/coacervates as phase-separated, micrometer-sized droplets,²⁵⁻²⁹ with recent work extended to cells.^{30,31}

Uniquely enabled by the single-molecule detection mechanism of SMdM, here we examine in aqueous solutions, in the low-concentration (~200 pM) limit of diffuser proteins, how interactor proteins of opposite and same charge signs, over wide concentration ranges, differently interact with the diffuser and thus modulate its translational diffusivity. This regime avoids the potential interferences of aggregate/coacervate formation, and thus better emulates how individual diffuser molecules interact with

the crowded, predominantly negatively charged intracellular environment. We thus document ubiquitous, net charge-driven nonspecific protein-protein interactions, wherein electrostatic attractions between species of opposite net charges substantially suppress diffusion. By converting the measured diffusivity to diffuser diameters, we further show that in the limit of excess interactors, a positively charged diffuser molecule effectively drags along a monolayer of negatively charged interactors, thus a model to elucidate the experimentally observed diffusion suppression of positively charged proteins in the living cell.

Results and discussion

We started by examining the diffusion of hen-egg-white lysozyme (HEWL) in a solution of bovine serum albumin (BSA). With an isoelectric point of ~10.7, the diffuser HEWL has an estimated net charge of +7 at the cytoplasmic pH of 7.3 (**Table S2**). Meanwhile, the interactor, the common protein standard BSA has an isoelectric point of ~5.0 and is -17 charged at pH 7.3 (**Table S2**).

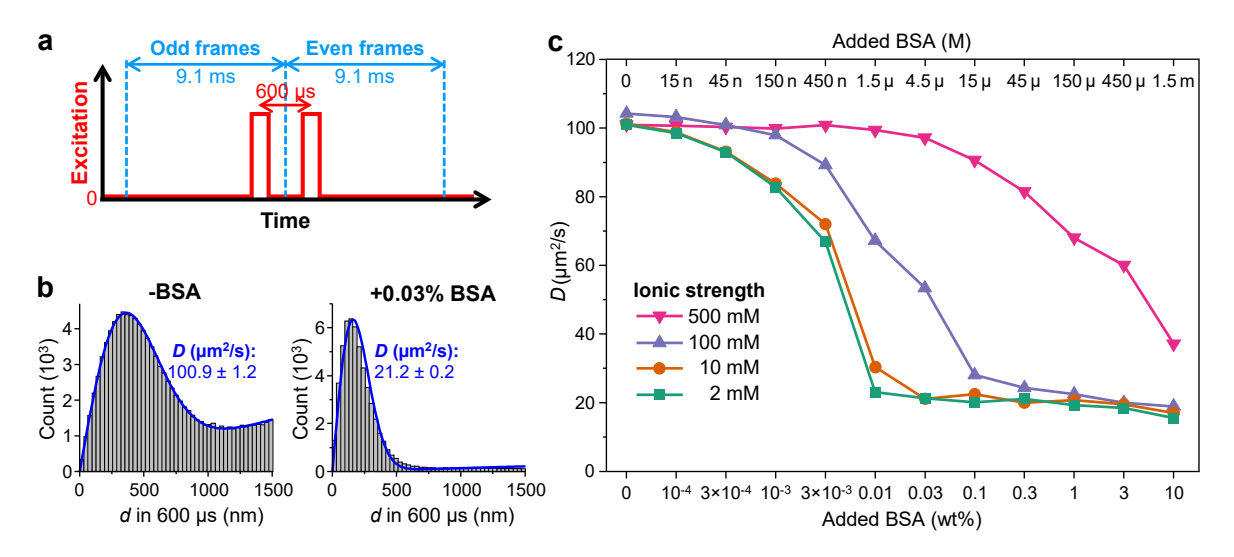


Fig. 1. Single-molecule diffusivity quantification unveils strong HEWL-BSA interactions in the low-concentration limit. (a) Schematics of the excitation sequence in SMdM, in which paired pulses were repeatedly applied across tandem camera frames to capture transient single-molecule displacements in the wide field over the time window defined by the pulse separation. (b) Example histograms of single-molecule displacements from SMdM, for 200 pM Cy3B-labeled HEWL diffusing in a pH = 7.3 buffer of 2 mM ionic strength, with and without the addition of 0.03% BSA. Blue lines: fits to the SMdM diffusion model, yielding diffusion coefficients *D* of 100.9±1.2 and 21.2±0.2 μm²/s (95% confidence intervals), respectively. (c) SMdM-determined *D* values for 200 pM Cy3B-labeled HEWL in pH = 7.3 buffers at ionic strengths of 2, 10, 100, and 500 mM, as a function of added BSA (bottom scale: weight percentage; top scale: molar concentration).

Fluorescently labeled HEWL was first diluted to $\sim\!200$ pM in a pH = 7.3 buffer. At this low concentration, the average distance between individual HEWL molecules in the solution was $\sim\!2$ µm, thus

permitting robust single-molecule detection and minimizing the likelihood of interactions between different HEWL molecules. For SMdM, an excitation laser repeatedly illuminated the sample as paired stroboscopic pulses across tandem camera frames at a fixed center-to-center separation of 600 μ s (**Fig. 1a**), thus enabling the rapid wide-field detection of $\sim 10^5$ transient single-molecule displacements for the 600 μ s time window in ~ 3 min (Methods). Fitting the accumulated single-molecule displacements to our diffusion model (**Fig. 1b** and Methods) yielded diffusion coefficient D with $\sim 1\%$ precisions. While the sub-millisecond time scale we probe does not resolve the individual transient interactions between biomolecules, it characterizes the averaged effects relevant to intracellular transports at sub-micrometer length scales.

For the starting 1 mM phosphate pH = 7.3 buffer (ionic strength ~2 mM), as well as buffers with KCl added to ionic strengths of 10, 100, and 500 mM, SMdM determined comparable D values of 101-104 μ m²/s for Cy3B-labeled HEWL (**Fig. 1b**). These values agree with our previous SMdM results, expected based on the 15 kDa molecular weight (**Fig. S1**).^{6,32}

Notably, as we added BSA to the sample, SMdM detected substantial drops in D in a concentration-dependent manner (**Fig. 1c**). In buffers of low ionic strengths of 2 and 10 mM, ~10% suppression in D was noted at 3×10^{-4} wt% (weight percentage), or 3 ppm (parts per million), addition of BSA. Note that 3 ppm BSA (45 nM) was still >200-fold over the ~200 pM concentration of the HEWL diffuser used in the measurement, and so interactions were not limited by the available amount of the BSA interactor in the solution. Increasing the BSA concentration to 0.01% (100 ppm; 1.5 μ M) suppressed the HEWL D values to <30 μ m²/s, and this value stabilized to ~20 μ m²/s for BSA concentrations of >0.03% (4.5 μ M). In comparison, the diffusivity of the Cy3B dye itself remained largely unaffected at >300 μ m²/s for BSA additions up to 1% (**Fig. S2**).

With the higher ionic strength of 100 mM, ~10% suppression in the D value of Cy3B-labeled HEWL was observed at 30 ppm (450 nM) BSA addition, and 300 ppm and 0.3% BSA additions suppressed the HEWL D values to ~50 and ~20 μ m²/s, respectively. For the very high ionic strength of 500 mM, diffusion suppression occurred at >~0.1% (15 μ M) BSA addition, with 1% and 10% BSA additions suppressing D to 68 and 38 μ m²/s, respectively.

To further elucidate the effects of ionic strength in this system, in another experiment, we initiated BSA-induced diffusion slowdown for HEWL in a 1 mM phosphate pH = 7.3 buffer, and then gradually added KCl to raise the ionic strength. SMdM detected HEWL diffusivity recovery in this process (**Fig.**

2a). Together, the observed ionic strength-dependent BSA suppression of HEWL diffusion suggests that the HEWL-BSA interaction is driven by electrostatic attractions and thus reversible when the protein charges are screened by high salts.

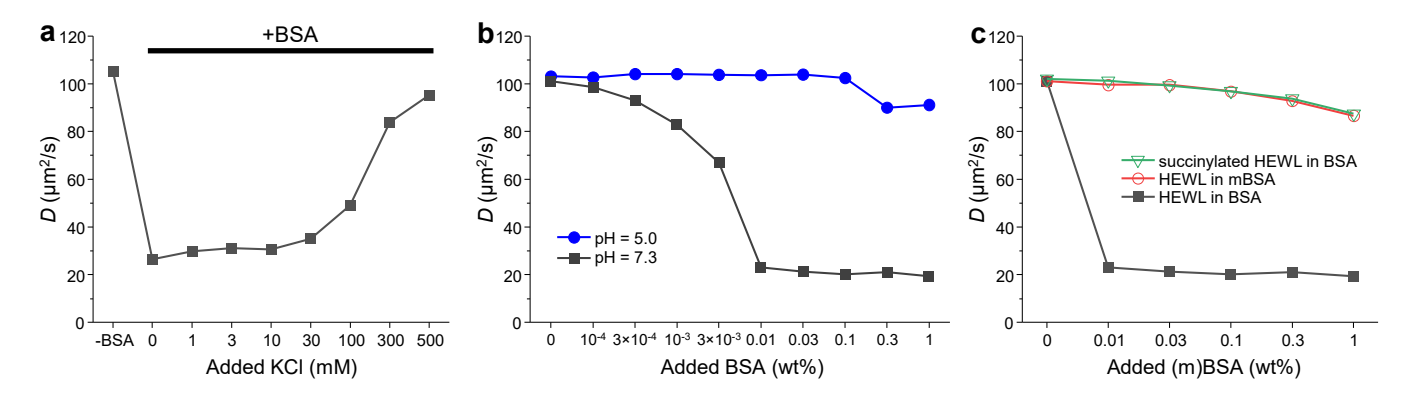


Fig. 2. The HEWL-BSA interaction is driven by electrostatic attractions based on the protein net charge. (a) SMdM-determined diffusion coefficient D for 200 pM Cy3B-labeled HEWL initially diffusing in a pH = 7.3 buffer of 2 mM ionic strength, to which 0.03% BSA and then KCl of different concentrations were sequentially added. (b) SMdM-determined D values for 200 pM Cy3B-labeled HEWL diffusing in 1 mM phosphate (pH = 7.3) or acetate (pH = 5.0) buffers, at different wt% of added BSA. (c) SMdM-determined D values in pH = 7.3 buffers of 2 mM ionic strength, for 200 pM Cy3B-labeled HEWL in the presence of varied wt% of methylated BSA (mBSA) (red) and 200 pM Cy3B-labeled succinylated HEWL (green) and HEWL (black) in the presence of varied wt% of BSA.

To directly probe the charge effects, we compared SMdM results in a 1 mM acetate buffer of pH = 5.0, the isoelectric point of BSA. We thus observed no changes in the HEWL diffusivity for BSA additions up to 0.1%, and only ~10% drops at higher BSA additions (**Fig. 2b**). These results corroborate our mechanism based on charge interactions, which vanished as BSA became neutral at its isoelectric point.

With the pH = 7.3 buffer, we further examined the diffusions of HEWL in methylated BSA (mBSA) and succinylated HEWL in BSA. These chemical modifications flip the net charges of BSA and HEWL to positive and negative, respectively.^{33,34} We thus found that for both systems, no appreciable suppression of diffusion occurred for up to 0.1% mBSA/BSA additions (**Fig. 2c**). ~10% *D* depressions were noted at 1% mBSA/BSA additions, attributable to slight increases in the solution viscosity. These results suggest negligible interactions between diffusers and interactors of the same charge signs. Together, SMdM showed that the BSA suppression of HEWL diffusion is driven by electrostatic attractions owing to the opposite net charges carried by the two proteins.

To generalize the above findings of electrostatic attraction-driven protein interactions, we next probed the diffusion of HEWL in the presence of the 45 kDa ovalbumin (isoelectric point: 4.5; estimated net charge at pH 7.3: -12), another common protein standard readily obtainable at bulk quantities. SMdM showed substantial, ionic strength-sensitive suppressions of diffusion as ovalbumin was added (**Fig. 3a**), similar to our results above with BSA addition.

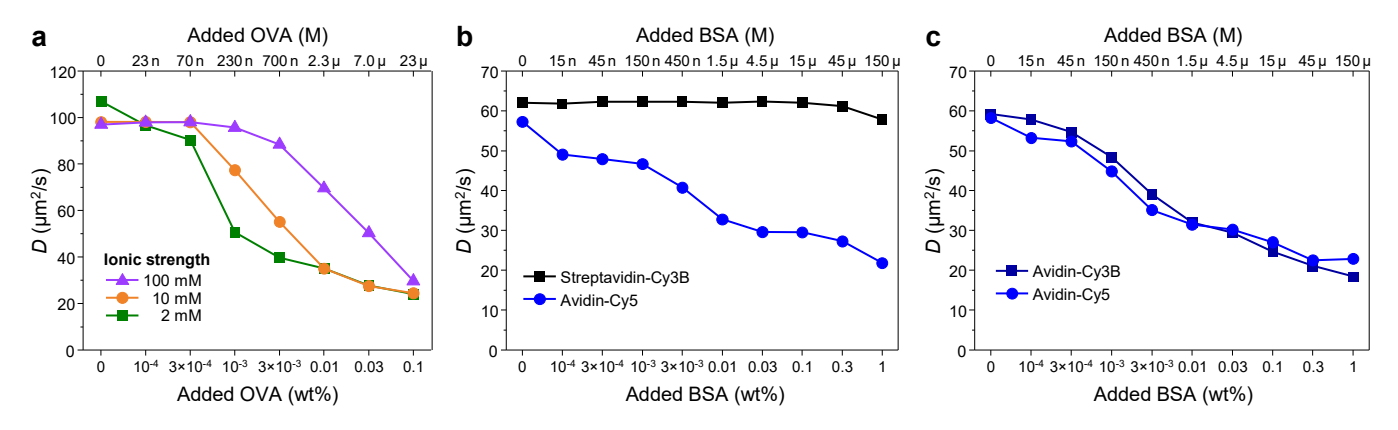


Fig. 3. Generalizing charge-driven interactions to HEWL-ovalbumin and avidin-BSA systems. (a) SMdM-determined diffusion coefficient *D* for 200 pM Cy3B-labeled HEWL in pH = 7.3 buffers at ionic strengths of 2, 10, and 100 mM, as a function of added ovalbumin (bottom scale: weight percentage; top scale: molar concentration). (b) Two-color SMdM *D* values for 200 pM Cy5-labeled avidin and 200 pM Cy3B-labeled streptavidin concurrently added to a pH = 7.3 buffer of 2 mM ionic strength, as a function of added BSA. (c) Two-color SMdM *D* values in another sample under similar conditions as (b), but with Cy3B-labeled avidin replacing Cy3B-labeled streptavidin.

In another assay, we compared the diffusion behaviors of avidin and streptavidin in BSA solutions. While similar in structure and both tightly bind biotin for bioconjugation applications, the ~68 kDa avidin tetramer has an isoelectric point of 10.5 and an ~+23 net charge at pH 7.3, whereas the ~60 kDa streptavidin tetramer has an isoelectric point of 6.4 and an estimated net charge of -4 at pH 7.3. Notably, as we separately labeled avidin and streptavidin with Cy5 and Cy3B and added both into the same sample to perform SMdM in two color channels, the addition of BSA suppressed diffusion of the former but not the latter (Fig. 3b). In comparison, in another sample in which Cy5- and Cy3B-labeled avidin were added into the same solution for two-color SMdM, similar diffusion suppressions by BSA were observed for both (Fig. 3c).

To further generalize the above net-charge-based interaction/noninteraction rules, we compared the diffusion of 8 different proteins (**Table S2**), each at \sim 200 pM concentration, in pH 7.3 buffers with varied BSA additions (**Fig. 4a**). Before adding BSA, the SMdM-determined D values of the different proteins (**Fig. S1**) showed molecule-weight dependences in excellent agreement with the Young-Carroad-

Bell model,³² consistent with our previous results.⁶ With BSA added, the 3 negatively charged proteins, Cy3B-labeled BSA, α-lactalbumin, and streptavidin, exhibited unvaried diffusivities up to 0.1% (15 μM) BSA addition and <10% suppressions at 1% (150 μM) BSA addition attributed to the aforementioned increases in solution viscosity. In contrast, the 4 substantially positively charged (>+5) proteins (Cy3B-labeled HEWL, CXCL9, avidin, and Histone H1.0) all exhibited markedly suppressed diffusion at ppm-level BSA additions, and converged to similar *D* values of ~20 μm²/s at >0.1% (15 μM) BSA levels. The mildly positively charged Cy3B-labeled RNase A (~+3 net charge) showed an intermediate behavior in which modest diffusion suppressions were observed for >0.01% (1.5 μM) BSA additions, with an ~40% suppression achieved at 1% (150 μM) BSA. Together, SM*d*M has demonstrated ubiquitous, nonspecific protein-protein interactions owing to electrostatic attractions between opposite net charges.

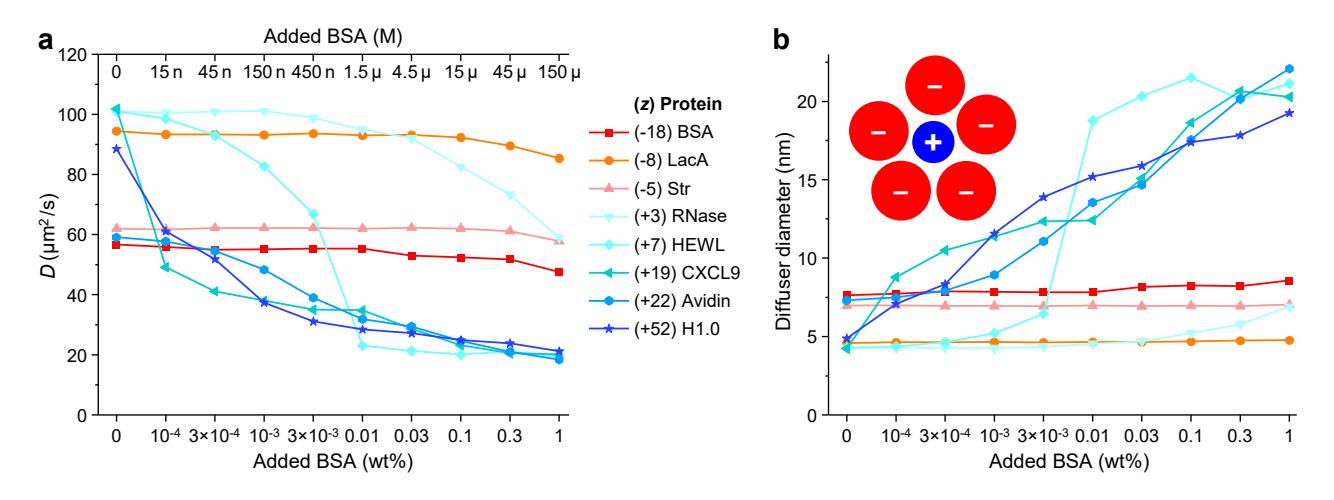


Fig. 4. SM*d*M survey of the diffusivity of different proteins in BSA solutions shows consistent slowdowns for positively charged species. (a) SM*d*M-determined diffusion coefficients D for 8 different Cy3B-labeled diffuser proteins separately added at 200 pM to pH = 7.3 buffers of 2 mM ionic strength, as a function of added BSA (bottom scale: weight percentage; top scale: molar concentration). The proteins are listed in the legend with their estimated net charge z. LacA, α-lactalbumin; Str, streptavidin; H1.0, Histone H1.0. See also Table S2. (b) Effective diffuser diameters (2× Stokes radii) of the different diffusers at different BSA concentrations, as converted from the D values in (a) through the Stokes-Einstein equation (methods). Inset model: A positively charged diffuser drags along a dynamic shell of negatively charged BSA interactors.

To rationalize the above curious convergence of D to ~20 μ m²/s at high BSA concentrations for the positively charged proteins, we converted the D values in Fig. 4a to effective diameters (2× Stokes radii) of the diffusers using the Stokes-Einstein equation (Methods). We thus found that as the differently sized diffuser proteins started with dissimilar diameters in the buffer, the negatively charged species maintained their effective diameters with BSA addition, whereas the positively charged species had their

effective diameters quickly grown and stabilized to ~17-22 nm for >0.1% (15 μ M) BSA additions (**Fig. 4b**). This size is ~3× the diameter of the interactor BSA (~7.5 nm based on our *D* values and previous studies), thus pointing to a model in which the positively charged diffuser, in the limit of low abundance, drags along a potentially dynamic shell of negatively charged BSA (**Fig. 4b inset**) to manifest a diffusion coefficient commensurate with that size.

As the positive net charge on a diffuser molecule is readily overcompensated by just a few BSA molecules, after the positive diffuser attracts a first layer of BSA interactors, the resultant dynamic complex will appear to the outside as being negatively charged. It is thus likely that electrostatic attraction stops right with the first BSA layer, which defines the apparent *D* of the diffuser regardless of further increases in BSA concentration. Before that limit is reached, how the *D* value evolves as a function of the interactor concentration may depend on the sizes and charge distributions of the diffuser and the interactor, awaiting future theoretical and experimental investigations. The low diffuser concentration allowed in SMdM measurements was instrumental in elucidating the above model, so that the amounts of the interactor remained in high excess over the diffuser throughout the measurement. It is thus unlikely for further complexing to occur through the interaction of multiple diffuser molecules with the same interactor molecule, a condition previously shown to generate micrometer-sized aggregates or coacervates when oppositely charged biomacromolecules are mixed at near equimolar ratios.^{25-28,30,31}

Conclusion

In conclusion, through SMdM, we have quantified how protein diffusion, in the limit of low diffuser concentrations, is modulated by differently charged interactor proteins over wide concentration ranges. We thus unveiled ubiquitous, net charge-driven protein-protein interactions and showed that in the limit of excess interactors, a positively charged diffuser molecule effectively drags along one monolayer of negatively charged interactors.

As the mammalian intracellular environment is dominated by negatively charged proteins^{5,11} and RNA counterbalanced by small cations (**Tabel S1**), the rarely encountered positively charged proteins would similarly drag along a dynamic shell of negatively charged macromolecules without further inducing aggregates or coacervates. The resultant complex thus provides an intuitive, refined model for the mechanism underlying the experimentally observed diffusion slowdown of positively charged proteins in the living cell. Intracellular macromolecular crowding, which progressively obstructs the diffusion of larger particles,^{2,22} conceivably further amplifies diffusion suppression, and such effects may be examined

in future studies. Interactions with cellular membranes, membrane proteins, and membrane-associated cytoskeletons,³⁵ as well as the diverse intraorganellar environments,¹¹ further add to the equation. Meanwhile, the demonstrated SMdM quantification of effective diffuser diameters opens new paths to elucidating molecular interactions through single-molecule detection.

Supporting Information

The Supporting Information is available free of charge on the ACS Publications website.

Materials and Methods; Accounting for molecular charges in the mammalian cytoplasm; List of proteins used in this work; SMdM-measured D values of the Cy3B-labeled proteins in Fig. 4 in the starting buffer; SMdM-measured D values of Cy3B in the presence of BSA (PDF)

Acknowledgment

We acknowledge support by the National Institute of General Medical Sciences of the National Institutes of Health (R35GM149349), the National Science Foundation (CHE-2203518), the Packard Fellowships for Science and Engineering, and the Heising-Simons Faculty Fellows Award.

References

- (1) Lippincott-Schwartz, J.; Snapp, E.; Kenworthy, A. Studying protein dynamics in living cells. *Nat. Rev. Mol. Cell Biol.* **2001**, *2*, 444-456.
- (2) Verkman, A. S. Solute and macromolecule diffusion in cellular aqueous compartments. *Trends Biochem. Sci.* **2002**, *27*, 27-33.
- (3) Machan, R.; Wohland, T. Recent applications of fluorescence correlation spectroscopy in live systems. *FEBS Lett.* **2014**, *588*, 3571-3584.
- (4) Lippincott-Schwartz, J.; Snapp, E. L.; Phair, R. D. The development and enhancement of FRAP as a key tool for investigating protein dynamics. *Biophys. J.* **2018**, *115*, 1146-1155.
- (5) Xiang, L.; Chen, K.; Yan, R.; Li, W.; Xu, K. Single-molecule displacement mapping unveils nanoscale heterogeneities in intracellular diffusivity. *Nat. Methods* **2020**, *17*, 524-530.
- (6) Choi, A. A.; Park, H. H.; Chen, K.; Yan, R.; Li, W.; Xu, K. Displacement statistics of unhindered single molecules show no enhanced diffusion in enzymatic reactions. *J. Am. Chem. Soc.* **2022**, *144*, 4839-4844.
- (7) Choi, A. A.; Xiang, L.; Li, W.; Xu, K. Single-molecule displacement mapping indicates unhindered intracellular diffusion of small (≤1 kDa) solutes. *J. Am. Chem. Soc.* **2023**, *145*, 8510-8516.
- (8) Park, H. H.; Choi, A. A.; Xu, K. Size-dependent suppression of molecular diffusivity in expandable hydrogels: A single-molecule study. *J. Phys. Chem. B* **2023**, *127*, 3333-3339.
- (9) He, C.; Wu, C. Y.; Li, W.; Xu, K. Multidimensional super-resolution microscopy unveils nanoscale surface aggregates in the aging of FUS condensates. *J. Am. Chem. Soc.* **2023**, *145*, 24240-24248.
- (10) Yan, R.; Chen, K.; Xu, K. Probing nanoscale diffusional heterogeneities in cellular membranes through multidimensional single-molecule and super-resolution microscopy. *J. Am. Chem. Soc.* **2020**, *142*, 18866-18873.

- (11) Xiang, L.; Yan, R.; Chen, K.; Li, W.; Xu, K. Single-molecule displacement mapping unveils sign-asymmetric protein charge effects on intraorganellar diffusion. *Nano Lett.* **2023**, *23*, 1711-1716.
- (12) Schavemaker, P. E.; Smigiel, W. M.; Poolman, B. Ribosome surface properties may impose limits on the nature of the cytoplasmic proteome. *eLife* **2017**, *6*, e30084.
- (13) Ye, Y.; Wu, Q.; Zheng, W.; Jiang, B.; Pielak, G. J.; Liu, M.; Li, C. Positively charged tags impede protein mobility in cells as quantified by ¹⁹F NMR. *J. Phys. Chem. B* **2019**, *123*, 4527-4533.
- (14) Leeb, S.; Sörensen, T.; Yang, F.; Mu, X.; Oliveberg, M.; Danielsson, J. Diffusive protein interactions in human versus bacterial cells. *Curr. Res. Struct. Biol.* **2020**, *2*, 68-78.
- (15) Leeb, S.; Yang, F.; Oliveberg, M.; Danielsson, J. Connecting longitudinal and transverse relaxation rates in live-cell NMR. *J. Phys. Chem. B* **2020**, *124*, 10698-10707.
- (16) Vallina Estrada, E.; Zhang, N.; Wennerström, H.; Danielsson, J.; Oliveberg, M. Diffusive intracellular interactions: On the role of protein net charge and functional adaptation. *Curr. Opin. Struct. Biol.* **2023**, *81*, 102625.
- (17) Beck, M.; Schmidt, A.; Malmstroem, J.; Claassen, M.; Ori, A.; Szymborska, A.; Herzog, F.; Rinner, O.; Ellenberg, J.; Aebersold, R. The quantitative proteome of a human cell line. *Mol. Syst. Biol.* **2011**, *7*, 549.
- (18) Itzhak, D. N.; Tyanova, S.; Cox, J.; Borner, G. H. H. Global, quantitative and dynamic mapping of protein subcellular localization. *eLife* **2016**, *5*, e16950.
- (19) Theillet, F. X.; Binolfi, A.; Frembgen-Kesner, T.; Hingorani, K.; Sarkar, M.; Kyne, C.; Li, C. G.; Crowley, P. B.; Gierasch, L.; Pielak, G. J. *et al.* Physicochemical properties of cells and their effects on intrinsically disordered proteins (IDPs). *Chem. Rev.* **2014**, *114*, 6661-6714.
- (20) Lodish, H. F.; Berk, A.; Kaiser, C.; Krieger, M.; Bretscher, A.; Ploegh, H. L.; Amon, A.; Martin, K. C. *Molecular cell biology*, Eighth edition. ed.; W.H. Freeman-Macmillan Learning: New York, 2016.
- (21) Wennerström, H.; Estrada, E. V.; Danielsson, J.; Oliveberg, M. Colloidal stability of the living cell. *Proc. Natl. Acad. Sci. U. S. A.* **2020**, *117*, 10113-10121.
- (22) Dix, J. A.; Verkman, A. S. Crowding effects on diffusion in solutions and cells. *Annu. Rev. Biophys.* **2008**, *37*, 247-263.
- (23) Rivas, G.; Minton, A. P. Macromolecular crowding *in vitro*, *in vivo*, and in between. *Trends Biochem. Sci.* **2016**, *41*, 970-981.
- (24) Guin, D.; Gruebele, M. Weak Chemical Interactions That Drive Protein Evolution: Crowding, Sticking, and Quinary Structure in Folding and Function. *Chem. Rev.* **2019**, *119*, 10691-10717.
- (25) Srivastava, S.; Tirrell, M. V. Polyelectrolyte complexation. Adv. Chem. Phys. 2016, 161, 499-544.
- (26) Croguennec, T.; Tavares, G. M.; Bouhallab, S. Heteroprotein complex coacervation: A generic process. *Adv. Colloid Interface Sci.* **2017**, *239*, 115-126.
- (27) Zheng, J.; Tang, C.-h.; Sun, W. Heteroprotein complex coacervation: Focus on experimental strategies to investigate structure formation as a function of intrinsic and external physicochemical parameters for food applications. *Adv. Colloid Interface Sci.* **2020**, *284*, 102268.
- (28) Kapelner, R. A.; Yeong, V.; Obermeyer, A. C. Molecular determinants of protein-based coacervates. *Curr. Opin. Colloid Interface Sci.* **2021**, *52*, 101407.
- (29) Galvanetto, N.; Ivanović, M. T.; Chowdhury, A.; Sottini, A.; Nüesch, M. F.; Nettels, D.; Best, R. B.; Schuler, B. Extreme dynamics in a biomolecular condensate. *Nature* **2023**, *619*, 876-883.
- (30) Zhu, Y.; Mohapatra, S.; Weisshaar, J. C. Rigidification of the *Escherichia coli* cytoplasm by the human antimicrobial peptide LL-37 revealed by superresolution fluorescence microscopy. *Proc. Natl. Acad. Sci. U. S. A.* **2019**, *116*, 1017-1026.
- (31) Yeong, V.; Werth, E. G.; Brown, L. M.; Obermeyer, A. C. Formation of Biomolecular Condensates in Bacteria by Tuning Protein Electrostatics. *ACS Cent. Sci.* **2020**, *6*, 2301-2310.

- (32) Young, M. E.; Carroad, P. A.; Bell, R. L. Estimation of diffusion coefficients of proteins. *Biotechnol. Bioeng.* **1980**, *22*, 947-955.
- (33) Saroff, H. A.; Rosenthal, N. R.; Adamik, E. R.; Hages, N.; Scheraga, H. A. The methylation of bovine serum albumin. *J Biol. Chem.* **1953**, *205*, 255-270.
- (34) Gitlin, I.; Carbeck, J. D.; Whitesides, G. M. Why are proteins charged? Networks of charge-charge interactions in proteins measured by charge ladders and capillary electrophoresis. *Angew. Chem. Int. Ed.* **2006**, *45*, 3022-3060.
- (35) Rentsch, J.; Bandstra, S.; Sezen, B.; Sigrist, P.; Bottanelli, F.; Schmerl, B.; Shoichet, S.; Noé, F.; Sadeghi, M.; Ewers, H. Sub-membrane actin rings compartmentalize the plasma membrane. *J. Cell Biol.* **2024**, *223*, e202310138.

Table of Contents (TOC)/Abstract Graphic

